Interdisciplinary Sciences: Computational Life Sciences (2023) 15:360–373
https://doi.org/10.1007/s12539-023-00560-4

ORIGINAL RESEARCH ARTICLE

A Novel Deep-Learning-Based CADx Architecture for Classification of Thyroid Nodules Using Ultrasound Images

Volkan Göreke[1]

Received: 10 October 2022 / Revised: 3 March 2023 / Accepted: 5 March 2023 / Published online: 28 March 2023

Abstract

Nodules of thyroid cancer occur in the cells of the thyroid as benign or malign types. Thyroid sonographic images are mostly used for diagnosis of thyroid cancer. The aim of this study is to introduce a computer-aided diagnosis system that can classify the thyroid nodules with high accuracy using the data gathered from ultrasound images. Acquisition and labeling of sub-images were performed by a specialist physician. Then the number of these sub-images were increased using data augmentation methods. Deep features were obtained from the images using a pre-trained deep neural network. The dimensions of the features were reduced and features were improved. The improved features were combined with morphological and texture features. This feature group was rated by a value called similarity coefficient value which was obtained from a similarity coefficient generator module. The nodules were classified as benign or malignant using a multi-layer deep neural network with a pre-weighting layer designed with a novel approach. In this study, a novel multi-layer computer-aided diagnosis system was proposed for thyroid cancer detection. In the first layer of the system, a novel feature extraction method based on the class similarity of images was developed. In the second layer, a novel pre-weighting layer was proposed by modifying the genetic algorithm. The proposed system showed superior performance in different metrics compared to the literature.

Graphical Abstract

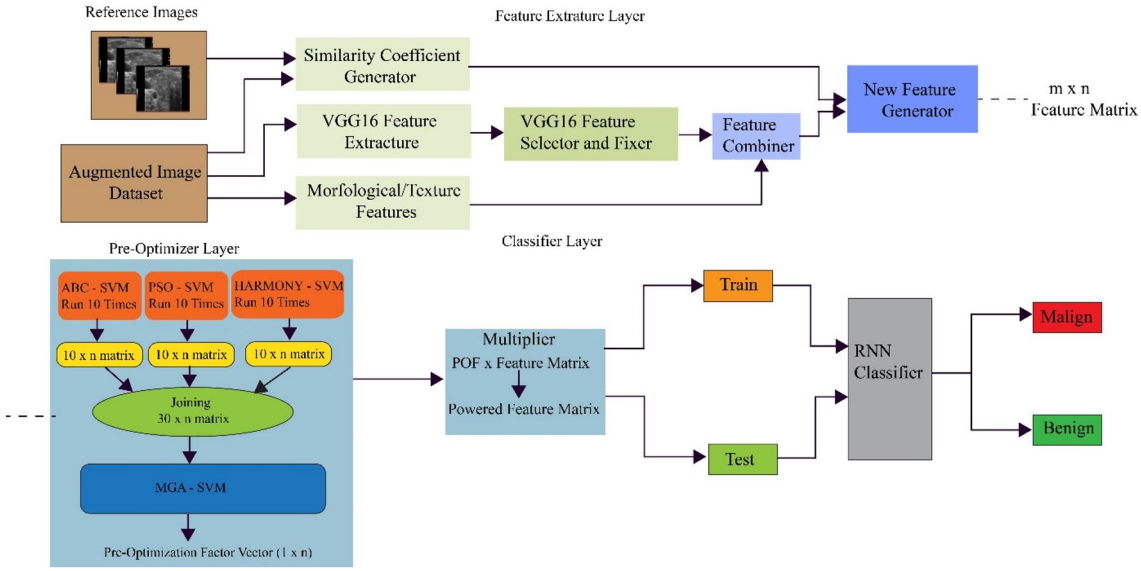

Keywords CADx · Thyroid nodules · Deep learning

✉ Volkan Göreke
vgoreke@cumhuriyet.edu.tr

Extended author information available on the last page of the article

1 Introduction

The abnormal growth of the thyroid cell tissue causes a benign (non-cancer) or malignant (cancer) type of nodule formation [1]. The specialists use "fine needle aspiration" or surgical methods for the diagnosis of these nodules. Although most of the thyroid tumors are benign, biopsy and surgery are applied to most of the patients one or more times. Besides, these methods require many resources such as staff and materials [2]. As an alternative method, specialists diagnose the disease by interpreting the ultrasound (US) images. American Radiology College (ACR) built a risk grading system called "ACR-Thyroid Imaging Reporting and Data System (TIRADS)" for interpretation of US images and categorization of nodules [3]. As an example, TIRADS 1 represents a benign nodule while TIRADS 5 represents a high-risk malignant nodule [4]. But the accuracy of the ultrasound-based diagnosis depends on the knowledge and experience of the radiologist and the quality of the sonography which causes errors on the diagnosis [5]. Therefore, computer-aided diagnosis (CAD) systems were developed to deal with the diagnosis errors. Such systems intend to reduce the interpretation errors by providing a second opinion in the specialist's decision process [6]. Deep learning (DL) is commonly used in the current CAD systems [7, 8, 9, 10] that were built for the diagnosis of thyroid nodule [11]. Li et al. introduced a DL approach based on R-CNN for the diagnosis of thyroid cancer [12]. Buda et al. implemented a DL architecture based on ResNet101 to obtain the nodule borders [13]. Li et al. tried to enhance the accuracy of the thyroid cancer detection in the ultrasound images using deep neural networks (DNN) [14]. Ma and Wu introduced a cascade DNN model for the segmentation of nodules [15]. Abdolali et al. introduced a DNN model based on masking for the detection of thyroid nodules [16].

In addition, there are segmentation studies performed for the detection of thyroid nodules in the literature. Koundal et al. [17] proposed a automated (fully) method based on intuitionistic fuzzy set for lesion segmentation on thyroid ultrasound images. Koundal et al. [18] introduced a method called "Spatial Neutrosophic Distance Regularized Level Set" (SNDRLS) for the identification of thyroid nodules. Li et al. [19, 20] proposed a deep active contour model for nodule segmentation. Li et al. [19, 20] introduced a Transformer and CNN-based method for the segmentation of malignant thyroid lesions. Koundal et al. [21] introduced a CAD system for segmentation of thyroid lesions on ultrasound images. Their proposed method performs both speckle noise removal and segmentation.

The determination of thyroid nodules using 3D high-resolution ultrasound (HRUS) images increases the accuracy of the diagnosis [22]. Acharya et al. obtained 100% accuracy, sensitivity, and specificity metrics using HRUS for the detection of thyroid cancer from ultrasound images [23]. In our study, the ultrasound dataset does not consist of 3D high-resolution images. Therefore, the study of Acharya et al. was not included in the comparison with the other works in the literature shown in Table 6. Thus, the performance of the study was evaluated objectively.

In this study, a novel multi-layer DL-based CAD architecture is proposed for the classification of thyroid nodules using US images. A novel feature extraction algorithm and a hybrid pre-weighting optimization layer were introduced to increase the classification accuracy in the proposed architecture. This study was organized under the following sections.

In Sect. 1, general descriptions for thyroid cancer and ultrasound imaging are given and the deep learning studies in the literature related with the ultrasound images and the thyroid cancer are examined. In Sect. 2, the methods and materials used in the study are explained in detail. In Sect. 3, the classifier layer and system performance testing approach are introduced. In Sect. 4, the achievement of the proposed architecture is measured using various metrics and the obtained results are compared with the literature. Section 5 is the conclusion part.

2 Materials and Methods

In this study, B-mode thyroid ultrasound images which were provided by Pedraza et al. via an open-access web application, were used. In this application, there are 33 benign images and 66 malignant images. Malignant classification was determined by the biopsy results. TI-RADS categories of images in each class were determined by the specialists and inserted into the database [24]. In this study, the segmentation of nodules was realized manually by a radiologist. In this study, a computer diagnostic system that diagnoses thyroid cancer on B-mode thyroid ultrasound images was proposed. The stages of the proposed system were developed as software using Matlab 2016 and "Visual Studio Community 2017 IDE Python Anaconda environment". The diagram given in Fig. 1 shows the architecture of the proposed system.

2.1 Medical Image Pre-processing

In the download page of the open-access database system, there are directories called "benign" and "malignant". There are sub-directories under each directory. These sub-directories contain an xml file and an ultrasound image belonging to a specific patient. The content of the xml file includes the coordinates of the nodule borders marked by the specialist and the information about the diagnosis provided by

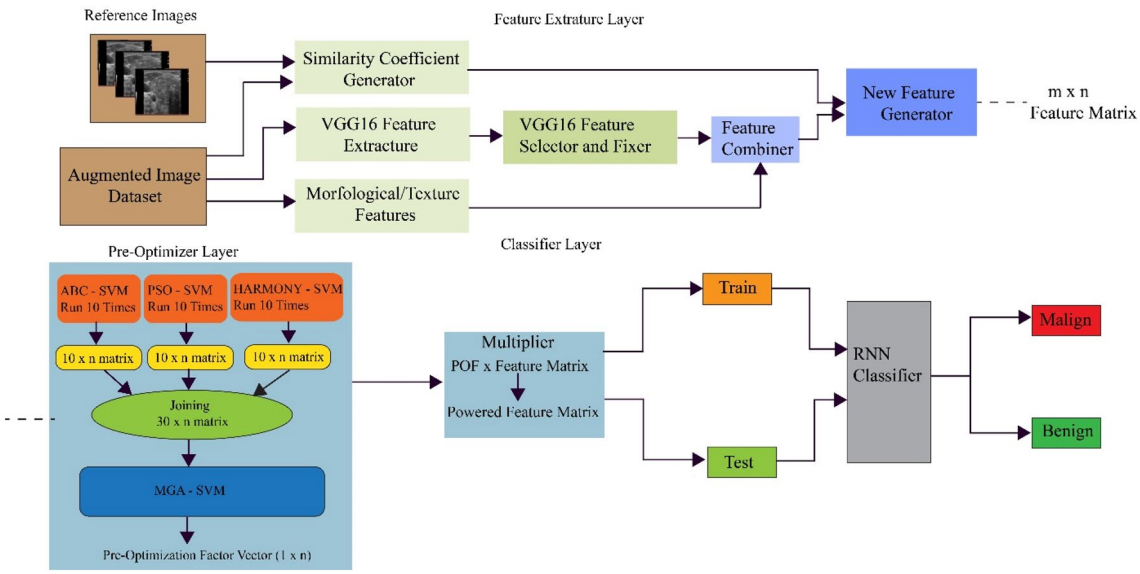

Fig. 1 Architectural diagram of the proposed system

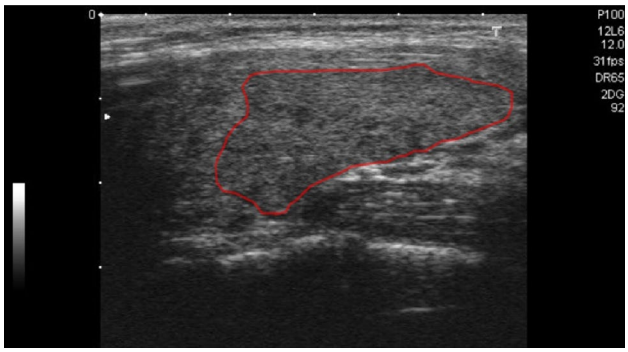

Fig. 2 Ultrasound image belonging to benign class

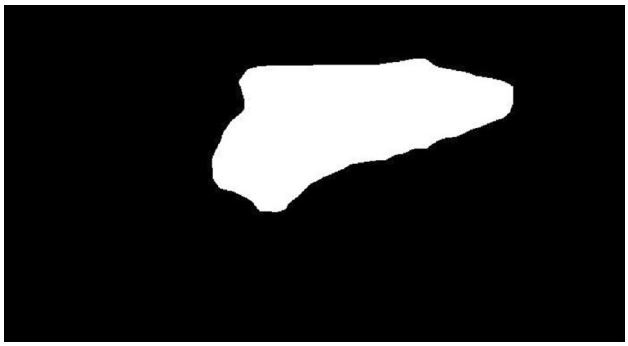

Fig. 3 Binary mask

the specialist. Unfortunately, some of these sub-directories only contain the xml file where the ultrasound images do not exist. Therefore, the ultrasound images were obtained manually by taking the screenshots of the web application. The borders of the nodules marked by the specialists can be seen in these images. The software developed using Matlab Image Processing Toolbox depends on the freehand mouse event. The coordinates of the nodule borders were easily obtained by the radiologist who can control the mouse by pressing the left button and moving it through a straight red line. Region of interest (ROI) was obtained using this coordinate information. Figure 2 shows a sample benign class and Fig. 3 shows the binary mask obtained after pre-processing phase.

2.2 Medical Image Data Augmentation

Small-scale datasets are one of the main problems that researchers face in medical imaging studies that depend on the artificial intelligence techniques. Data augmentation method which depends on minor variations on the images is a method used to deal with this problem [25, 26]. But you should be careful not to lose the descriptive features of the nodules while applying such methods. For example, rotation of the image may not be suitable because the shadow can never be seen in the reverse direction of ultrasound rays [22]. Zing et al. indicate that the death risk increases depending on the size of the tumor. According to this study, zooming the ultrasound image would not be a suitable data augmentation technique because it would change the tumor size [27]. Suitable data augmentation techniques are given in Table 1. These techniques were applied using ImageDataGenerator class of Keras library in Python environment and a total of 1188 synthetic image data were obtained.

In this study, 33 original images of benign class were named as reference images and were not included in the augmented dataset to be able to evaluate the study

Table 1 Image data augmentation techniques

Technique	Parameter
Width shift range	− 0.01, 0.01
Height shift range	− 0.01, 0.01
Shear range	0.1, 0.2, 0.3, 0.4
Brightness range	0.2–1.5 (0.2–0.5, 0.2–0.8, 0.6–1.0, 1.0–1.5)

more objectively. This method depends on the similarity between images; therefore, having same images in both reference image dataset and training dataset would increase the performance but would not provide an objective evaluation. The dataset containing 1254 images (396 benign images and 858 malignant images with 66 original malignant images) were obtained.

2.3 Similarity Coefficient Generator

Usually, mean square error (*MSE*), peak signal-to-noise ratio (*PSNR*), structural similarity index measure (*SSIM*) metrics are used to measure the structural information similarity between the reference image and the compared image [28–30]. Mathematical equations of these metrics are given in Eqs. 1, 2 and 3.

Here, f and g are images of same size (MxN). μ_f and μ_g are the mean of the pixels in the images, σ_f, σ_g standard deviation and σ_{fg} is the covariance value between images, *C1*, *C2*, and *C3* are constants [31].

$$MSE(f,g) = \frac{1}{MN}\sum_{i=1}^{M}\sum_{j=1}^{N}\left(f_{ij} - g_{ij}\right)^2 \tag{1}$$

$$PSNR(f,g) = 10\log_{10}\left(255^2 / MSE(f,g)\right) \tag{2}$$

$$SSIM(f,g) = \left(\frac{2\mu_f\mu_g + C_1}{\mu_f^2\mu_g^2 + C_1}\right)\cdot\left(\frac{2\sigma_f\sigma_g + C_2}{\sigma_f^2\sigma_g^2 + C_2}\right)\cdot\left(\frac{\sigma_{fg} + C_3}{\sigma_f\sigma_g + C_3}\right) \tag{3}$$

Algorithm 1 was implemented to obtain Similarity Coefficient (*sc*) value where IR(1), IR(2), IR(3),…, IR(33) represent reference images and ID(1), ID(2), ID(3),…, ID(1254) represent the images in the dataset. Similarity Measurement Method (*SMM*) is used for performance evaluation. For example, *SMM(f, g) = MSE(f, g)* means that MSE will be calculated between images. *SV* represents the similarity vector of size 1 × 33.

Algorithm 1. Similarity Coefficient Generator

```
Begin:
For i=1:size(image data set) Do
    f=Read Image (ID(i))
    For j=1:size(reference image dataset) Do
    g= Read Image (IR (j))
    SMM={MSE(f,g),PSNR (f,g),SSIM(f,g)}
        For idx=1:size(SMM) Do
            SV{idx}(i,j)= SMM{idx}(f,g)
        End For
    End For
End for
Save values;
SV{1}=i x 33 similarity matrix using MSE  // here i equals the image dataset size
SV{2}=i x 33 similarity matrix using PSNR
SV{3}=i x 33 similarity matrix using SSIM
Calculate the mean/standard deviation/variance foreach row of the matrices
Vstd{1 to 3}=standard mean(SV{1 to 3})
Vmean{1 to 3} = mean (SV{1 to 3})
Vvar{1 to 3} = variance(SV{1 to 3})
Generate i x 9 Vm matrix by combining Vstd{1 to 3},Vmean{1 to 3},Vvar{1 to 3}
Determining the most discriminative feature among the values obtained by three statistical
calculations (mean, standard variation, variance)
Choose statistical method using SPSS;
Apply distribution test (Kolmogorov–Smirnov) on Vm matrix
    "Student's t test for normal distributions"
    "Mann–Whitney U test for abnormal distributions"
Apply suitable statistical test to the Vm matrix using SPSS and calculate p value
Select Similarity Coefficient vector (depending on p value) of size 1254 x 1, sc
End
```

This algorithm was run individually for *MSE*, *PSNR*, and *SSIM* methods and *sc* values were calculated. The most discriminative method and the statistical value were determined via the statistical tests applied using SPSS [32, 33]. The tests showed that the most discriminative value (having the smallest *p* value) was the variance calculated using *SSIM* method.

2.4 VGG16 Feature Extraction

The convolutional neural networks (CNNs) are complex, multi-layer DNN that contain the trained filters and pooling in its architecture [34]. VGG16 architecture is a CNN model that was proposed by Simonyan and Zisserman [35].

Transfer learning is a machine learning technique and is based on the transfer of learning parameters. The goal of this method is to reuse a DNN model pre-trained with a dataset with large amount of data in another classification and feature extraction task [36]. In practice, a pre-trained CNN which was trained with a dataset with large amount of samples is trained again with a smaller dataset.

ImageNet is a natural image dataset that contains more than 14 million images. This dataset was used in the literature as a pre-training dataset for neural network studies that contain medical images [25].

Neural network models that depend on DL are quite commonly used in the literature for classification of medical images. In most of these studies, medical images are provided as inputs of the deep neural network for classification tasks [37]. In this study, medical images are not directly applied to the classifier. Initially, VGG16 deep neural network was pre-trained using ImageNet dataset. Then deep numerical features were obtained from the thyroid US images using pre-trained VGG16.

In this study, the strategy while choosing the pre-trained DNN was to prefer the model with the lowest performance [38]. Thus, the power of the proposed method is presented more objectively. Otherwise the performance of the pre-trained model would affect the system performance and the superiority of the proposed method would not be presented objectively.

Figure 4 shows the proposed VGG-16 architecture. In this architecture, the section from the Conv 1–1 layer to the pooling layer was separated and used for feature extraction. As a result, a deep feature vector of size $7 \times 7 \times 512$ is obtained from an input image. Depending on the dimensions of the augmented ultrasound dataset, 1254 feature vectors of size $7 \times 7 \times 512$ were obtained.

2.5 VGG16 Feature Selector and Fixer

The large data size is a problem for classification algorithms. Such data increase both computational cost and memory usage. Furthermore, a reduction in the feature space causes a more comprehensible model and will have a positive effect on the classification power [29, 30]. Therefore, only 20 of 25.088 ($7 \times 7 \times 512$) features obtained from VGG16 model in the previous stage were selected for each image. Chi2 method was used in feature selection process which implements a statistical significance between label values and classes. This process was implemented using "sklearn.feature_selection" python module in an Anaconda environment.

After this process, a feature matrix of size 1254×20 was obtained. But when the feature vectors of different classes are analyzed, it can be seen that zero value has been produced too many times. Having the same values in the feature vectors of different classes (especially for the features having the same indices in the feature vectors) decreases the classification performance by negatively effecting the discrimination of the classifier. Algorithm 2 was implemented to deal with this case. The main goal of this algorithm is to replace the zero-valued features in the feature vector with the maximum-valued element in that vector. This was called the feature fixer in Fig. 1.

Algorithm 2. Feature Fixer

```
Num=Read feature matrix // Num: m x n size matrix
For i=1 to size(Num[row]) Do
    Numtemp(1,:)=Num(i,:) // Num(i,:) i: row all column
    Mak=maximum(Numtemp)
    For j= 1 to size(Num[column]) Do
        If Numtemp == 0
            New(i,j)=Mak
        Else
            New(i,j)=Num(i,j)
        End If
    End For
End For
```

2.6 Morphological/Texture Feature

There are some specific points in the process where specialists examine the ultrasound images for diagnosis. For example, in the medical literature, echotexture is a specific concept related with the infrastructure of the nodule [39]. This concept corresponds to the texture analysis method in image processing. Usually, the statistical features depending on the histograms containing grey level or the grey level coexistence matrices are constructed using such analysis [40]. The structural view of the nodule in the ultrasound image is another discriminative point [41]. Morphological

Fig. 4 VGG-16 architecture

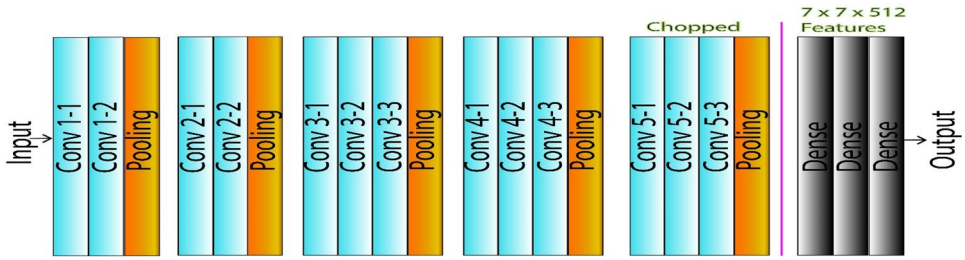

analysis is realized to extract the structural features of the nodule such as margin and shape [42].

In this study, four texture features called contrast, energy, homogeneity, and correlation and six morphological features called area, axis rate, form factor, roundness, aspect, and perimeter were extracted.

Grey-Level Co-Occurrence Matrix (GLCM) depends on the estimation of the second-order compound state probability density function $P_d(x, y| m, z)$. This matrix represents the transition probability from grey level x to grey level y when the distance between the pixels is m and the angle between the pixels is z [43]. Contrast, which is a measure of pixel density, is also a measure of local variations in the image. Energy is the measure of irregularity in the image texture. It uses a measurement method based on the repetition of pixel pairs. Homogeneity is inversely proportional with the contrast and it measures the regularity of grey level distribution. Correlation measures the linear dependency of pixel pair grey levels [44]. The number of pixels within the borders of the nodules in the medical image is called the area. The feature called *LtoS* is calculated by dividing the long axis of the nodule to the short axis. Perimeter is the total number of pixels that generate the nodule borders. Roundness is the ratio of the area to the long axis. Form factor is calculated by dividing the 4 times *pi* value to the square of the perimeter value. The aspect value is calculated by a ratio operation. It is obtained by dividing the pixel area covering the nodule by the surrounding pixel length of that nodule [45].

In this part of the study, a total of ten morphological and texture features were extracted. By applying a *t*-test (Mann–Whitney *U* test) using SPSS; contrast, energy, homogeneity, correlation, area and roundness which are significantly discriminative ($p < 0.05$) were defined as the feature group among many features.

2.7 Feature Combiner and New Feature Generator

The feature matrix of size 1254×20 obtained from VGG16 architecture and the morphological/texture feature group of size 1254×6 were combined and a feature matrix of size 1254×26 was obtained with a process called feature combiner. *f* represents the feature parameter. The calculation performed by New Feature Generator is given mathematically in Eq. 4 for $n = 1, 2, 3, \ldots, 26$ and $m = 1, 2, 3, \ldots, 1024$.

Table 2 Performance comparison of optimization algorithms

Performance	Worst	Best	Mean	Std mean
ABC-SVM	96,20,319	97,60,159	96,73,705	0.457669
PSO-SVM	96,00,797	97,20,319	96,40,637	0.452503
HAR-SVM	95,60,956	96,80,478	96,08,765	0.429097
MGA-SVM	96,80,478	97,60,159	97,46,879	0.255105

$$\text{New Feature Matrix} = \begin{bmatrix} \frac{f_{11}}{sc_1} & \frac{f_{12}}{sc_1} & \frac{f_{13}}{sc_1} & \cdots & \frac{f_{1n}}{sc_1} \\ \frac{f_{21}}{sc_2} & \frac{f_{22}}{sc_2} & \frac{f_{23}}{sc_2} & \cdots & \frac{f_{2n}}{sc_2} \\ \cdot & \cdot & & & \cdot \\ \cdot & \cdot & & & \cdot \\ \frac{f_{m1}}{sc_m} & \frac{f_{m2}}{sc_m} & \frac{f_{m3}}{sc_m} & \cdots & \frac{f_{mn}}{sc_m} \end{bmatrix} \tag{4}$$

2.8 Pre-optimizer Layer

Goreke et al. designed a pre-weighting layer based on ABC optimization algorithm in the classifier architecture proposed for the prediction of COVID-19 [46]. In this study, a novel pre-weighting layer called Pre-optimizer Layer was implemented based on the previously mentioned pre-weighting layer. At the output of this layer, a pre-weighting vector of size $1 \times n$ consisting of pre-weighting coefficients is obtained. This vector is called the Pre-optimization Factor Vector (*POF*) in Fig. 1.

In genetic algorithm, having an efficient initial population plays a significant role in the solution of the problem [47]. Even the initial population is randomly generated in most of the genetic algorithm studies, there are some methods for generating an initial population [48, 49]. In this study, a novel method was proposed to generate the initial population. The steps of this method are given in Algorithm 3.

The cascade architecture of Pre-Optimizer Layer was designed on the principle of running the SVM algorithm inside the optimization algorithms (ABC, SVM, HARMONY). The accuracy parameter (*Acc*) which is a performance measure of the SVM classifier, was used as the cost functions of the optimization algorithms. The mathematical equation of the accuracy parameter is given in Eq. 5. Here, true positive (*TP*) and true negative (*TN*) represent the number of malignant and benign classes that are correctly classified; false positive (*FP*) and false negative (*FN*) represent the number of malignant and benign classes that are wrongly classified [50].

Optimization algorithms use the function given in Eq. 6 as the fitness function (*Obj*). Each optimization algorithm is used for searching the optimum values of pre-weighting coefficients ($s_1, s_2, s_3, \ldots, s_n$).

$$Acc_{SVM} = \frac{TP + TN}{TP + FP + FN + TN} \tag{5}$$

$$Obj = (1/Acc) \tag{6}$$

Table 3 Deep neural network architectures and hyper parameters

Parameter	ANN	CNN	RNN	LSTM
Unit	32-16-8	512-256	–	–
Layers	1-2-3	1-2	1	1
Activation function	ReLU	ReLU	ReLU	ReLU
Learning rate	1e–3	1e–3	1e–3	1e–3
Loss function	Binary cross entropy	Binary cross entropy	Binary cross entropy	Binary cross entropy
Epocs	250	250	250	250
Optimizer	SGD	SGD	SGD	SGD
Decay	1e–5	1e–5	1e–5	1e–5
Momentum	0.3	0.3	0.3	0.3
Full conn.unit	–	2048-1024-512	2048-1024-512	2048-1024-512
Full conn.layer	–	1-2-3	1-2-3	1-2-3
RNN unit	–	–	512	
LSTM unit	–	–	–	512
Dropout	–	0.25	0.25	

Table 4 The performances of DL classifiers with diverse architectures

Classifier	Acc	Recall	Precision	F1-score	AUC
ANN	0.9927	0.9927	0.9927	0.9927	1
CNN	0.9991	0.9991	0.9991	0.9991	1
LSTM	0.9981	0.9981	0.9981	0.9981	1
RNN	0.9995	0.9995	0.9995	0.9995	1

Acc accuracy, *AUC* area under the curve

$$Data\ Set\ Matrix\ for\ SVM = \begin{bmatrix} s_1 \times \frac{f_{11}}{sc_1} & s_2 \times \frac{f_{12}}{sc_1} & s_3 \times \frac{f_{13}}{sc_1} & \dots & s_n \times \frac{f_{1n}}{sc_1} \\ s_1 \times \frac{f_{21}}{sc_2} & s_2 \times \frac{f_{22}}{sc_2} & s_3 \times \frac{f_{23}}{sc_2} & \dots & s_n \times \frac{f_{2n}}{sc_2} \\ . & . & . & & \\ . & . & . & & \\ s_1 \times \frac{f_{m1}}{sc_m} & s_2 \times \frac{f_{m2}}{sc_m} & s_3 \times \frac{f_{m3}}{sc_m} & \dots & s_n \times \frac{f_{mn}}{sc_m} \end{bmatrix} \tag{7}$$

Algorithm 3. Steps of initial population generation for modified genetic algorithm

Step 1. Run ABC-SVM 10 times and generate matrix1 (10 x n)

Step 2. Run PSO-SVM 10 times and generate matrix2 (10 x n)

Step 3. Run Harmony-SVM 10 times and generate matrix3 (10 x n)

Step 4. Combine matrix1, matrix2 and matrix3 and generate 30 x n matrix (initial population for genetic algorithm)

Using this method, the initial population of the genetic algorithm was generated from the optimum values obtained from three different optimization algorithms. The reason to use the genetic algorithm as the final optimizer in this layer is that it contains the natural selection and crossover mechanisms in its structure. Because even if one of the optimization algorithms generate the best performing pre-weighting vector, some of the coefficients in this vector may not be the optimal values. Similarly, it is also possible that there can be a coefficient with the optimal value inside the vector generated by a worse performing algorithm. The best performing vector that contains the optimal values can be obtained with the crossover and natural selection mechanisms that already exist in the nature of genetic algorithm. The mutation phase of the genetic algorithm is realized by generating a random value between the minimum- and maximum-valued genes inside the chromosome. The standard genetic algorithm is given in Algorithm 4. The individual performances of the optimization algorithms with the SVM classifier are shown in Table 2. The accuracy parameter of the SVM classifier was used as the performance metric. Every method was repeated 20 times using different initial population values. Then worst, best, mean values, and standard deviation were calculated. As shown in Table 2, the best performance was obtained with the modified genetic algorithm proposed in this study.

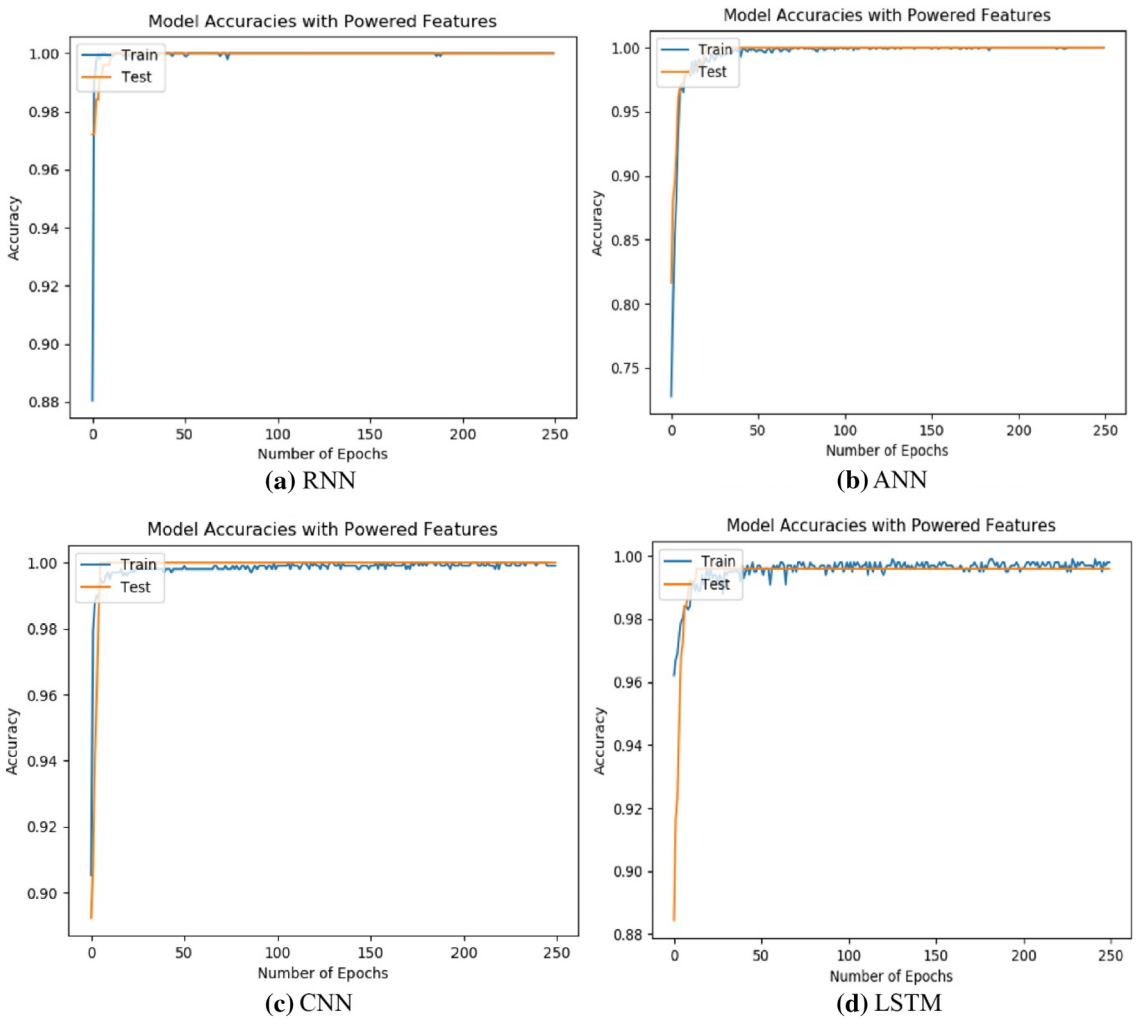

Fig. 5 Model accuracy graphs of the classifiers **a** RNN classifier **b** ANN classifier **c** CNN classifier **d** LSTM classifier

Algorithm 4. Standard genetic algorithm

```
Begin
    Create initial population;
    While (Until Stooping Criteria)    Do
        For (Each Choromosome) Do
            Calculate fitness value;
            Selection (Survival of strong individuals)
            If (There are same choromosones)
            Mutation (Changing some genes for new and different individuals);
            End If
        End For
    Generate new population
    End While
End
```

The accuracy value of the Support Vector Machine classifier constitutes the cost function for the generation of Pre-Optimization Factor Vector (*POF*) given in Fig. 1. The *POF* vector is obtained as a result of running the modified genetic algorithm that tries to minimize the reverse of the cost function.

3 Classifier Layer and System Performance Test Approach

The New Feature Matrix given by Eq. 4 in the Multiplier section (Fig. 1), is weighted with the pre-weighting coefficients (p_1, p_2, p_3, …, p_n) that generate the *POF* vector. The numerical dataset obtained after this process is called Power Feature Matrix and is represented mathematically by Eq. 8.

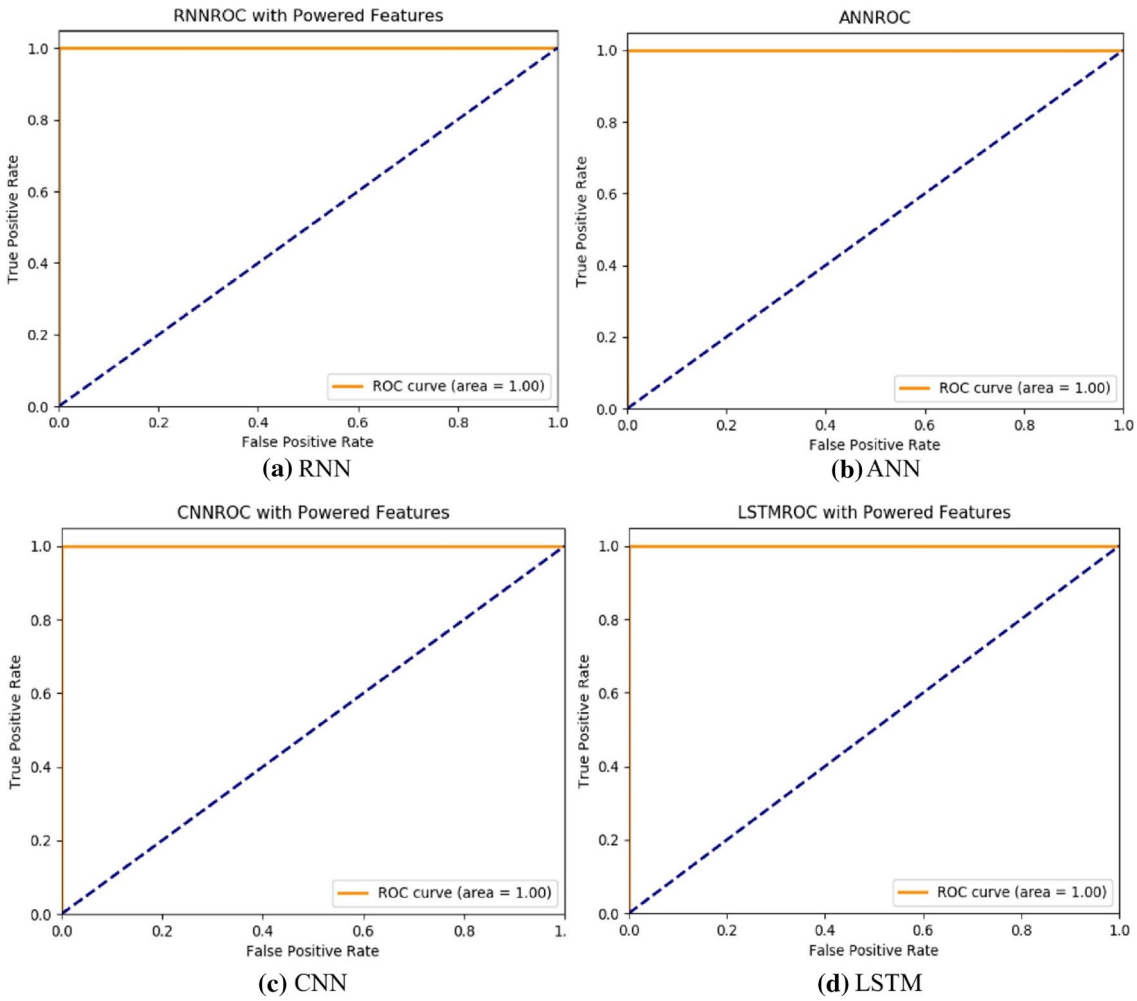

Fig. 6 ROC graph of the classifiers **a** RNN classifier **b** ANN classifier **c** CNN classifier **d** LSTM classifier

$$Powered\ Feature\ Matrix = \begin{bmatrix} p_1 \times \frac{f_{11}}{sc_1} & p_2 \times \frac{f_{12}}{sc_1} & p_3 \times \frac{f_{13}}{sc_1} & \dots & p_n \times \frac{f_{1n}}{sc_1} \\ p_1 \times \frac{f_{21}}{sc_2} & p_2 \times \frac{f_{22}}{sc_2} & p_3 \times \frac{f_{23}}{sc_2} & \dots & p_n \times \frac{f_{2n}}{sc_2} \\ . & . & . & & \\ . & . & . & & \\ p_1 \times \frac{f_{m1}}{sc_m} & p_2 \times \frac{f_{m2}}{sc_m} & p_3 \times \frac{f_{m3}}{sc_m} & \dots & p_n \times \frac{f_{mn}}{sc_m} \end{bmatrix} \tag{8}$$

Various deep neural network architectures used in this study and their hyper parameters are shown in Table 3.

The train-test split approach which produces cleaner results especially in the clinical applications, is chosen as the deep-learning training strategy [51].

4 Results and Discussion

In this study, the performances of the proposed multi-layered classifier architecture and the powered feature matrix were measured using the metrics defined between Eqs. 9 and 12.

$$Accuracy = (TP + TN)/(TP + TN + FP + FN) \tag{9}$$

$$Recall = TP/(TP + FN) \tag{10}$$

$$Precision = TP/(TP + FP) \tag{11}$$

$$F1 - score = 2 \times precision \times recall/precision + recall \tag{12}$$

Furthermore, receiving operating characteristic (*ROC*) curve was used to calculate *AUC* (area under the curve) [52].

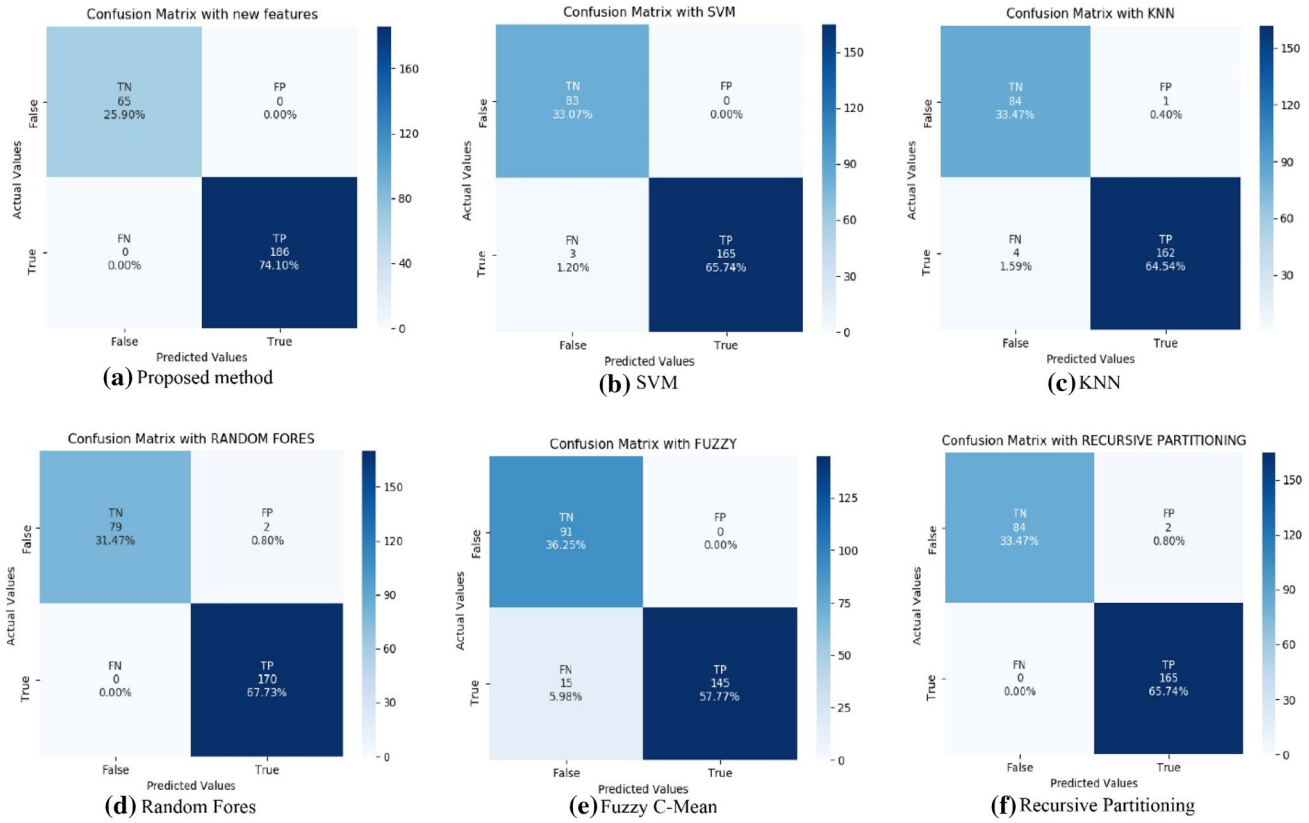

Fig. 7 The confusion matrices of the proposed method and other methods

The performances of DL classifiers with diverse architectures are given in Table 4.

These results are the average of the results obtained over the test data in each epoc in the training process of the deep neural network.

After the experiments, RNN architecture with the highest accuracy was chosen as the deep learning classifier. The model accuracy graphs and ROC graphs of the classifiers are given in Figs. 5 and 6.

Figure 5 is given to reveal the validity and reliability of the model, and Fig. 6 is given to reveal the performance of the model at all classification thresholds [46]. In addition, the graphical representation of the performances obtained from other methods in the literature is given in Fig. 7 using confusion matrices [46].

Table 5 The effect of Algorithm 2 on the system performance

Algorithm 2	Acc	Recall	Precision	F1-score	AUC
Non used	0.9992	0.9992	0.9992	0.9992	1
Used	0.9995	0.9995	0.9995	0.9995	1

In addition, to examine the effect of Algorithm 2 on the proposed system, a dataset was created by bypassing Algorithm 2 and applied to the RNN classifier layer.

Obtained performance results are given in Table 5. According to the results in Table 5, Algorithm 2 contributes positively to the average performance of the system.

The performance of the proposed method was compared with the studies in the literature and the results are given in Table 6. Additionally, the performance comparison of the studies performed with the same dataset used in this study is given in Table 7.

For Table 6, the graph was created according to the accuracy parameters of the studies in the literature given in Fig. 8.

5 Conclusion

In this study, a novel DL-based CAD design that classifies the thyroid nodule as “benign” or “malignant” from the thyroid US images, having a better accuracy than the studies in the literature, was proposed.

Table 6 Performance comparison of proposed method and the literature works

No	References	Method	Other metrics (%)	Accuracy (%)
1	Ding et al. [53]	SVM	Sen = 94.6 Spec = 92.6	93.6
2	Acharya et al. [23]	KNN	Sen = 98 Spec = 99.8 ROC = 98.7	98.9
3	Acharya et al. [54]	SVM-FUZZY	–	98.1
4	Acharya et al. [55]	FUZZY	–	99.6
5	Raghavendra et al. [56]	SVM	Sen = 90.32 Spec = 98.57 AUC = 94.45	97.52
6	Chi et al. [57] (Dataset-2)	CNN—Random Forest	Sen = 86 Spec = 99	96.34
7	Mugasa et al. [6]	Random Forest and Recursive Partitioning Classifiers	Sen = 99.64 Spec = 90.23	96
8	Ma et al. [15]	CNN	Sen = 82.41 Spec = 84.41 AUC = 89	83.02
9	Seo et al. [58]	AlexNet	Sen = 71.05 Spec = 93.19 AUC = 89.5	89.52
10	Song et al. [59]	ResNet-18/ImageNet	Sen = 93.96 Spec = 92.68	93.75
11	Ma et al. [15]	Cascade CNN	AUC = 98.51	–
12	Pedraza et al. [24]	VGG16/ImageNet	Precision = 88.08 Recall = 90.08	–
13	Ying et al. [60]	Multi-layer CNN	Precision = 99.74 Recall = 98.62 F1-score = 99.18	99.47
14	Kang et al. [61]	Multi-stage multi-task learning	F1-score = 89.15 AUC = 96.08	90.75
15	Proposed method	Multi-layer RNN	Recall = 99.95 Precision = 99.95 F1-score = 99.95 AUC = 1.00	99.95

In this study, an algorithmic method based on the statistical computation was developed for putting forth the structural similarity between benign and malign images. The software module called the Similarity Coefficient Generator generates the value called the Similarity Coefficient (*sc*).

Images are directly applied to the classifier, in most of the studies in the literature related with the classification of medical images using deep neural networks. In this study, a different approach was introduced. Initially, the numerical feature data were extracted from the images using a pre-trained VGG16 network and the size of the numerical feature data was reduced using chi2 method for having a positive effect on the classification performance. Then the zero-valued elements of each feature vector in the reduced feature data matrix were replaced with the maximum value of that vector using the designed algorithm. Thus, the decrease in the classification accuracy because of having the same values (zero values) with the same indices in the vectors of different classes, was tried to be resolved.

In the literature review, no study was found that dealt with this aspect of the subject.

Table 7 Comparison of the proposed method with literature studies using the same dataset

References	Method	Other metrics	Accuracy (%)
Zhu et al. [36, 62]	ResNet-18	Sen = 93.96 spec = 92.68	93.75
Chi et al. [57]	Random Forest classifier	Sen = 99.1 spec = 93.90	98.29
Nguyen et al. [63]	Modified Resnet	Sen = 94.92 spec = 63.74	90.88
Proposed method	Multi-layer RNN	Recall = 99.95 Precision = 99.95 f1-score = 99.95 AUC = 1.00	99.95

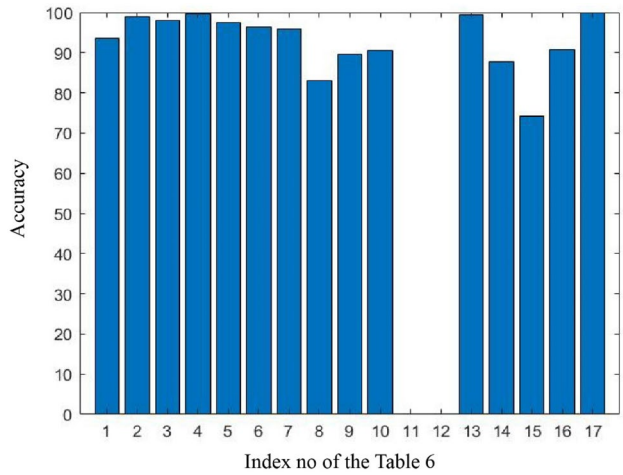

Fig. 8 Accuracy performance graph of literature studies

The texture and morphological features were extracted with the suggestion of the specialist, the significant ones (according to the *p* value) were chosen and added to the numerical feature vector obtained from VGG16 network.

In this study, a novel pre-optimization method with a high accuracy was developed by modifying the genetic algorithm for the CAD system. An approach with a performance better than the combined ABC-SVM pre-optimization method of Ref. [46] was introduced.

In this study, the proposed DL-based multi-layer classifier architecture was compared with the studies that used various artificial intelligence methods, and different metrics were provided to demonstrate that the proposed architecture shows a superior performance.

Furthermore, the studies that used the same dataset with this study were also compared and it was proved that the proposed approach has a better classification accuracy.

Supplementary Information The online version contains supplementary material available at https://doi.org/10.1007/s12539-023-00560-4.

Acknowledgements Thanks to Dr. Oğuz Karabörklü who is a radiologist working at Sivas Numune Hospital for realizing the computer segmentation of the thyroid lesion areas in the ultrasound images.

Data Availability The dataset used in this work was obtained from open-access databases. The access address of the dataset is given below in the manuscript. http://cimalab.unal.edu.co/applications/thyroid/.

Declarations

Conflict of Interest The author confirms that there are no known conflicts of interest associated with this publication.

References

1. Sree SV, Ph D, Molinari F, Ph D, Gupta S, Ph D, Bardales RH, Witkowska A, Aimbe F (2014) A review on ultrasound-based thyroid cancer tissue characterization and automated classification. Technol Cancer Res Treat 13(4):289–301. https://doi.org/10.7785/tcrt.2012.500381
2. Galbraith JD, Swann N, Cox B, Letendre N, Recabaren J (2018) The bethesda classification for thyroid fine needle aspiration: a predictor or an alarmist? Am Surg 84(1):161–164. https://doi.org/10.1177/000313481808400140
3. Anand V, Koundal D (2020) Computer-assisted diagnosis of thyroid cancer using medical ımages: a survey. In: Singh P, Kar A, Singh Y, Kolekar M, Tanwar S (eds) Proceedings of ICRIC 2019. Lecture notes in electrical engineering, vol 597. Springer, Cham. https://doi.org/10.1007/978-3-030-29407-6_39
4. Tessler FN et al (2017) ACR Thyroid Imaging, Reporting and Data System (TI-RADS): White Paper of the ACR TI-RADS Committee. J Am Coll Radiol 14(5):587–595. https://doi.org/10.1148/37.6.755
5. Koundal D, Gupta S, Singh S (2012) Applications of neutrosophic and intuitionistic fuzzy set on image processing, İn: National Conference on GreenTechnologies: Smart and Efficient Management (GTSEM-2012). SLIET, Longowal, pp 1–4
6. Mugasa H, Dua S, Koh JEW, Hagiwara Y, Shu O, Madla C, Kongmebhol P, Hoong K, Acharya UR (2020) An adaptive feature extraction model for classification of thyroid lesions in ultrasound images. Pattern Recogn Lett 131:463–473. https://doi.org/10.1016/j.patrec.2020.02.009
7. Arirangan S, Kottursamy K (2021) Multi-scaled feature fusion enabled convolutional neural network for predicting fibrous dysplasia bone disorder. Expert Syst. https://doi.org/10.1111/exsy.12882
8. Saranya A, Kottursamy K, AlZubi AA, Bashir AK (2022) Analyzing fibrous tissue pattern in fibrous dysplasia bone images using deep R-CNN networks for segmentation. Soft Comput 26(16):7519–7533. https://doi.org/10.1007/s00500-021-06519-1
9. Sollini M, Cozzi L, Chiti A, Kirienko M (2018) Texture analysis and machine learning to characterize suspected thyroid nodules and differentiated thyroid cancer: where do we stand? Eur J Radiol 99(November 2017):1–8. https://doi.org/10.1016/j.ejrad.2017.12.004
10. Xu L, Gao J, Wang Q, Yin J, Yu P, Bai B, Pei R, Chen D, Yang G, Wang S, Wan M (2020) Computer-aided diagnosis systems in diagnosing malignant thyroid nodules on ultrasonography: a systematic review and meta-analysis. Eur Thyroid J 9(4):186–193. https://doi.org/10.1159/000504390
11. Chu C, Zheng J, Zhou Y (2021) Computer Methods and Programs in Biomedicine Ultrasonic thyroid nodule detection method based on U-Net network. Comput Methods Programs Biomed 199:105906. https://doi.org/10.1016/j.cmpb.2020.105906
12. Li H, Weng J, Shi Y, Gu W, Mao Y, Wang Y, Liu W (2018) An improved deep learning approach for detection of thyroid papillary cancer in ultrasound images. Sci Rep. https://doi.org/10.1038/s41598-018-25005-7
13. Buda M, Tessler FN (2019) Management of thyroid nodules seen on US ımages : deep learning may match performance of radiologists. Radiology. https://doi.org/10.1148/radiol.2019181343
14. Li X, Zhang S, Zhang Q, Wei X, Pan Y, Zhao J, Xin X, Qin C, Wang X, Li J, Yang F (2019) Articles Diagnosis of thyroid cancer using deep convolutional neural network models applied to sonographic images: a retrospective, multicohort, diagnostic

study. Lancet Oncol 20(2):193–201. https://doi.org/10.1016/S1470-2045(18)30762-9
15. Ma J, Wu F (2017) Cascade convolutional neural networks for automatic detection of thyroid nodules in ultrasound images. Med Phys. https://doi.org/10.1002/mp.12134
16. Abdolali F, Kapur J, Jaremko JL, Noga M, Hareendranathan AR, Punithakumar K (2020) Automated thyroid nodule detection from ultrasound imaging using deep convolutional neural networks. Comput Biol Med 122(March):103871. https://doi.org/10.1016/j.compbiomed.2020.103871
17. Koundal D, Sharma S, Guo Y (2020) Intuitionistic based segmentation of thyroid nodules in ultrasound images. Comput Biol Med 121:103776. https://doi.org/10.1016/j.compbiomed.2020.103776
18. Koundal D, Gupta S, Singh S (2016) Automated delineation of thyroid nodules in ultrasound images usingspatial neutrosophic clustering and level set. Appl Soft Comput 40(2016):86–97. https://doi.org/10.1016/j.asoc.2015.11.035
19. Li Z, Zhou S, Chang C, Wang Y, Guo Y (2023) A weakly supervised deep active contour model for nodule segmentation in thyroid ultrasound images. Pattern Recogn Lett 165:128–137. https://doi.org/10.1016/j.patrec.2022.12.015
20. Li G, Chen R, Zhang J, Liu K, Geng C, Lyu L (2023) Fusing enhanced Transformer and large kernel CNN for malignant thyroid nodule segmentation. Biomed Signal Process Control 83:104636. https://doi.org/10.1016/j.bspc.2023.104636
21. Koundal D, Gupta S, Singh S (2018) Computer aided thyroid nodule detection system using medical ultrasound images. Biomed Signal Process Control 40:117–130. https://doi.org/10.1016/j.bspc.2017.08.025
22. Sharifi Y, Amin M, Dehghani T (2021) Deep learning on ultrasound images of thyroid nodules. Biobybernetics Biomed Eng 41:636–655. https://doi.org/10.1016/j.bbe.2021.02.008
23. Acharya UR, Faust O, Sree SV, Molinari F, Suri JS (2011) ThyroScreen system: high resolution ultrasound thyroid image characterization into benign and malignant classes using novel combination of texture and discrete wavelet transform. Comput Methods Programs Biomed 107(2):233–241. https://doi.org/10.1016/j.cmpb.2011.10.001
24. Pedraza L, Vargas C, Romero E (2015) An open access thyroid ultrasound-image database. https://doi.org/10.1117/12.2073532
25. Pérez-garcía F, Sparks R, Ourselin S (2021) TorchIO: a Python library for efficient loading, preprocessing, augmentation and patch-based sampling of medical images in deep learning. Comput Methods Programs Biomed 208:106236. https://doi.org/10.1016/j.cmpb.2021.106236
26. Shi G, Wang J, Qiang Y, Yang X, Zhao J, Hao R, Yang W, Du Q, Kazihise NG (2020) Computer Methods and Programs in Biomedicine Knowle dge-guide d synthetic medical image adversarial augmentation for ultrasonography thyroid nodule classification. Comput Methods Programs Biomed 196:105611. https://doi.org/10.1016/j.cmpb.2020.105611
27. Zhang J, Cheng X, Su B, Wang X, Wang L (2020) The increased risk of thyroid cancer-specific mortality with tumor size in stage IVB patients. Front Oncol 10(November):1–11. https://doi.org/10.3389/fonc.2020.560203
28. Wang H, Maldonado D, Silwal S (2011) A nonparametric-test-based structural similarity measure for digital images. Comput Stat Data Anal 55(11):2925–2936. https://doi.org/10.1016/j.csda.2011.04.021
29. Wang J, Chen P, Zheng N, Chen B, Principe JC, Wang F (2021) Neurocomputing Associations between MSE and SSIM as cost functions in linear decomposition with application to bit allocation for sparse coding. Neurocomputing 422:139–149. https://doi.org/10.1016/j.neucom.2020.10.018
30. Wang Z, Wang C, Wei J, Liu J (2021) Knowledge-based systems multi-class feature selection by exploring reliable class correlation. Knowl Based Syst 230:107377. https://doi.org/10.1016/j.knosys.2021.107377
31. Horé A (2010) Image quality metrics: PSNR vs. SSIM Image quality metrics: PSNR vs. SSIM. August. https://doi.org/10.1109/ICPR.2010.579
32. Lo CM, Chang YC, Yang YW, Huang CS, Chang RF (2015) Quantitative breast mass classification based on the integration of B-mode features and strain features in elastography. Comput Biol Med 64:91–100. https://doi.org/10.1016/j.compbiomed.2015.06.013
33. Moon WK, Lo C, Chang JM (2013) Quantitative ultrasound analysis for classification of BI-RADS category 3 breast masses. J Digit Imaging 26:1091–1098. https://doi.org/10.1007/s10278-013-9593-8
34. Ji S, Xu W, Yang M, Yu K (2013) 3D convolutional neural networks for human action recognition. IEEE Trans Pattern Anal Mach Intell 35(1):221–231. https://doi.org/10.1109/TPAMI.2012.59
35. Simonyan K, Zisserman A (2015) Very deep convolutional networks for large-scale image recognition. 3rd ınternational conference on learning representations, ICLR 2015—conference track proceedings, pp 1–14. https://arxiv.org/abs/1409.1556.
36. Zhu J, Wang X, Kou L, Zheng L, Zhang H (2021) Applied surface science application of combined transfer learning and convolutional neural networks to optimize plasma spraying. Appl Surf Sci 563(October 2020):150098. https://doi.org/10.1016/j.apsusc.2021.150098
37. Ashraf R, Habib MA, Akram M, Latif MA, Sheraz M, Malik A, Awais M, Dar SH, Mahmood T, Yasir M, Abbas Z (2020) Deep convolution neural network for big data medical image classification. IEEE Access 8:105659–105670. https://doi.org/10.1109/ACCESS.2020.2998808
38. Brodzicki A, Jaworek-korjakowska J, Kleczek P (2020) Pretrained deep convolutional neural network for clostridioides difficile bacteria cytotoxicity classification based on fluorescence ımages. Sensors. https://doi.org/10.3390/s20236713
39. Anil G, Hegde A, Chong FHV (2011) Thyroid nodules: risk stratification for malignancy with ultrasound and guided biopsy. Cancer Imaging 11:209–223. https://doi.org/10.1102/1470-7330.2011.0030
40. Pereira R, Zanchetta M, Cesar D (2012) Expert systems with applications texture extraction: an evaluation of ridgelet, wavelet and co-occurrence based methods applied to mammograms. Expert Syst Appl 39(12):11036–11047. https://doi.org/10.1016/j.eswa.2012.03.020
41. Kim E, Park CS, Oh KK, Kim DI, Lee JT, Yoo HS (2002) New sonographic criteria for recommending fine-needle aspiration biopsy of nonpalpable solid nodules of the thyroid. AJR Am J Roentgenol 178:687–691. https://doi.org/10.2214/ajr.178.3.1780687
42. Iwanowski M, Skoneczny S (2014) Image features extraction using mathematical morphology. https://doi.org/10.1117/12.279581
43. Haralick RM, Dinstein I, Shanmugam K (1973) Textural features for ımage classification. IEEE Trans Syst Man Cybern SMC-3(6):610–621. https://doi.org/10.1109/TSMC.1973.4309314
44. Mall PK, Singh PK, Yadav D (2019) GLCM based feature extraction and medical X-ray ımage classification using machine learning techniques
45. Uzunhisarcıklı E, Goreke V (2018) A novel classifier model for mass classification using BI-RADS category in ultrasound images based on Type-2 fuzzy inference system. Sādhanā 43(9):138. https://doi.org/10.1007/s12046-018-0915-x
46. Göreke V, Sarı V, Kockanat S (2021) A novel classifier architecture based on deep neural network for COVID-19 detection using

laboratory findings. Appl Soft Comput J 106:107329. https://doi.org/10.1016/j.asoc.2021.107329
47. Deng Y, Liu Y, Zhou D (2015) An ımproved genetic algorithm with ınitial population strategy for symmetric TSP. Math Probl Eng 2015:1–6. https://doi.org/10.1155/2015/212794
48. Chen J, Zhang S, Gao Z, Yang L (2010) Feature-based initial population generation for the optimization of job shop problems. J Zhejiang Univ Sci C 11(10):767–777. https://doi.org/10.1631/jzus.C0910707
49. Sharma D, Deb K (2011) Domain-specific initial population strategy for compliant mechanisms using customized genetic algorithm. Struct Multidisc Optim 43:541–554. https://doi.org/10.1007/s00158-010-0575-x
50. Mumtaz W, Qayyum A (2019) A deep learning framework for automatic diagnosis of unipolar depression. Int J Med Informatics 132(September):103983. https://doi.org/10.1016/j.ijmedinf.2019.103983
51. Alakus TB, Turkoglu I (2020) Comparison of deep learning approaches to predict COVID-19 infection. Chaos Solitons Fractals 140:110120. https://doi.org/10.1016/j.chaos.2020.110120
52. Pierce R (2009) Evaluating information: validity, reliability, accuracy and triangulation. Retrieved March 21, 2017. https://www.sagepub.com/sites/default/files/upm-binaries/17810_5052_Pierce_Ch07.pdf. https://doi.org/10.4135/9780857024589.D12
53. Ding J, Cheng H, Ning C, Huang J, Zhang Y (2011) Quantitative measurement for thyroid cancer characterization based on elastography. J Ultrasound Med 30(9):1259–1266. https://doi.org/10.7863/jum.2011.30.9.1259
54. Acharya UR, Sree SV, Krishnan MM, Molinari F, Garberoglio R, Suri JS (2012) Non-invasive automated 3D thyroid lesion classification in ultrasound: a class of ThyroScan™ systems. Ultrasonics 52(4):508–520. https://doi.org/10.1016/j.ultras.2011.11.003
55. Acharya UR, Sree SV, Swapna G, Gupta S, Molinari F, Garberoglio R, Witkowska A, Suri JS (2013) Effect of complex wavelet transform filter on thyroid tumor classification in three-dimensional ultrasound. Proc Inst Mech Eng [H] 227(3):284–292. https://doi.org/10.1177/0954411912472422
56. Raghavendra U, Acharya UR, Gudigar A, Tan JH, Fujita H, Hagiwara Y, Molinari F, Kongmebhol P, Ng KH (2017) Fusion of spatial gray level dependency and fractal texture features for the characterization of thyroid lesions. Ultrasonics 77:110–120. https://doi.org/10.1016/j.ultras.2017.02.003
57. Chi J, Walia E, Babyn P, Wang J, Groot G, Eramian M (2017) Thyroid nodule classification in ultrasound images by fine-tuning deep convolutional neural network. J Digit Imaging 30:477–486. https://doi.org/10.1007/s10278-017-9997-y
58. Seo JK, Kim YJ, Kim KG, Shin I, Shin JH, Kwak JY (2017) Differentiation of the follicular neoplasm on the gray-scale US by image selection subsampling along with the marginal outline using convolutional neural network. BioMed Res Int 2017:3098293. https://doi.org/10.1155/2017/3098293
59. Song W, Li S, Liu J, Qin H, Zhang B, Zhang S, Hao A (2019) Multitask cascade convolution neural networks for automatic thyroid nodule detection and recognition. IEEE J Biomed Health Inform 23(3):1215–1224. https://doi.org/10.1109/JBHI.2018.2852718
60. Ying X, Yu Z, Yu R, Li X, Yu M, Zhao M, Liu K (2018) Thyroid nodule segmentation in ultrasound images based on cascaded convolutional neural network. In: Cheng L, Leung A, Ozawa S (eds) Neural information processing. ICONIP 2018. Lecture notes in computer science, vol 11306. Springer, Cham, pp 373–384
61. Kang Q, Lao Q, Li Y, Jiang Z, Qiu Y, Zhang S, Li K (2022) Thyroid nodule segmentation and classification in ultrasound images through intra- and inter-task consistent learning. Med Image Anal 79:102443. https://doi.org/10.1016/j.media.2022.102443
62. Zhu Y, Fu Z, Fei J (2017) An image augmentation method using convolutional network for thyroid nodule classification by transfer learning. In: 2017 3rd IEEE international conference on computer and communications (ICCC). https://doi.org/10.1109/CompComm.2017.8322853
63. Nguyen DT, Kang JK, Pham TD, Batchuluun G, Park KR (2020) Ultrasound image-based diagnosis of malignant thyroid nodule using artificial intelligence. Sensors 20(7):1822. https://doi.org/10.3390/s20071822

Authors and Affiliations

Volkan Göreke[1]

[1] Department of Computer Technologies, Sivas Vocational School of Technical Sciences, Sivas Cumhuriyet University, 58140 Sivas, Türkiye

Editors

Andreas Goerling, University of Erlangen-Nuremberg, Germany
Xinqi Gong, Renmin University of China, Beijing, China 2023.7.31加入
Gerrit C. Groenenboom, Nijmegen Radboud Universiteit, Netherlands
Ruoxu Gu, Shanghai Jiao Tong University, Shanghai, China
Hong Guo, University of Tennessee, Knoxville, USA
Jonathan D. Hirst, University of Nottingham, Nottingham, UK
Philip Hoggan, Universite Clermont II, Clermont, France
Jian Huang, University of Electronic Science and Technology of China,Chengdu, China
Zuyi Huang, Biotechnology High Performance Computing Software Applications Institute (BHSAI), Frederick, USA
Zunnan Huang, Guangdong Medical University, Dongguan, China
Guangfu Ji, Chinese Academy of Engineering Physics, Mianyang, China
Kirk Jordan, IBM, Armonk, New York, USA
Sabre Kais, Purdue University, West Lafayette, USA
Mihaly Kállay, Budapest University of Technology and Economics, Budapest, Hungary
Maria Kurnikova, Carnegie Mellon University, Pittsburgh, USA
Xiujuan Lei, Shaanxi Normal University, Xi'an, China
William A. Jr. Lester, University of California, Berkeley, USA
Min Li, Central South University, Changsha, China
Carmay Lim, Institute of Biomedical Sciences, Academia Sinica, Taipei, China
Jian Liu, Nankai University, Shanghai, China
Robert Moszynski, University of Warsaw, Warsaw, Poland
Masha Niv, The Hebrew University of Jerusalem, Jerusalem, Israel
Louis Noodleman, The Scripps Research Institute, La Jolla, USA
Gilles H. Peslherbe, Concordia University, Montreal, Canada
Piotr Piecuch, Michigan State University, East Lansing, USA
Jean-Philip Piquemal, Université Pierre et Marie Curie, Paris, France
Xianghong Hanna Qi, Oak Ridge National Laboratory, Oak Ridge, USA
Stuart Rothstein, Brock University, St. Catharines, Canada
Bairong Shen, Sichuan University, Chengdu, China
Shigenori Tanaka, Kobe University, Kobe, Japan
David J Tozer, Durham University, Durham, UK
Jack Tuszynski, University of Alberta, Edmonton, Canada
Yan Alexander Wang, University of British Columbia, Vancouver, Canada
Donald Weaver, Dalhousie University, Nova Scotia, Canada
Leyi Wei, Shandong University, Jinan, China
Yanjie Wei, Shenzhen Institutes of Advanced Technology, Shenzhen, China
Tomasz A. Wesolowski, University of Geneva, Geneva, Switzerland
Hongyan Wu, Shenzhen Institutes of Advanced Technology, Shenzhen, China
Chuanle Xiao, Sun Yat-sen University,Guangzhou, China
Yi Xiong, Shanghai Jiao Tong University, Shanghai, China
Yuedong Yang, Sun Yat-sen University, Guangzhou, China
Jianyang Zeng, Westlake University, Hangzhou, China
Wen Zhang, Huazhong Agricultural University, Wuhan, China
Yujuan Zhang, Chongqing Normal University, Chongqing, China
Qi Zhao, University of Science and Technology Liaoning, Anshan, China
Meng Zhou, Wenzhou Medical University, Wenzhou, China
Quan Zou, University of Electronic Science and Technology of China, Chengdu, China
Yongchun Zuo, Inner Mongolia University, Hohhot, China

Master Journal List | Search Journals | Match Manuscript | Downloads | Help Center | Login | Create Free Account

Already have a manuscript?

Use our Manuscript Matcher to find the best relevant journals!

Find a Match

Filters | Clear All

Web of Science Coverage

Open Access

Category

Country / Region

Refine Your Search Results

Interdisciplinary Sciences Computational Life Sciences | Search | Sort By: Relevancy

Search Results

Found 20,680 results (Page 1) Share These Results

Did you mean this journal?

INTERDISCIPLINARY SCIENCES-COMPUTATIONAL LIFE SCIENCES

Publisher: SPRINGER HEIDELBERG , TIERGARTENSTRASSE 17, HEIDELBERG, GERMANY, D-69121

ISSN / eISSN: 1913-2751 / 1867-1462

Web of Science Core Collection: Science Citation Index Expanded

Additional *Web of Science* Indexes: Biological Abstracts | BIOSIS Previews | Essential Science Indicators

2022 Journal Performance Data for: Interdisciplinary Sciences-Computational Life Sciences

ISSN
1913-2751

EISSN
1867-1462

JCR ABBREVIATION
INTERDISCIP SCI

ISO ABBREVIATION
Interdiscip. Sci.

Journal Information

EDITION
Science Citation Index Expanded (SCIE)

CATEGORY
MATHEMATICAL & COMPUTATIONAL BIOLOGY - SCIE

LANGUAGES
English

REGION
CHINA MAINLAND

1ST ELECTRONIC JCR YEAR
2013

Publisher Information

PUBLISHER
SPRINGER HEIDELBERG

ADDRESS
TIERGARTENSTRASSE 17, D-69121 HEIDELBERG, GERMANY

PUBLICATION FREQUENCY
4 issues/year

Rank by Journal Impact factor

Journals within a category are sorted in descending order by Journal Impact Factor (JIF) resulting in the Category Ranking below. A separate rank is shown for each category in which the journal is listed in JCR. Data for the most recent year is presented at the top of the list, with other years shown in reverse chronological order. Learn more

EDITION

Science Citation Index Expanded (SCIE)

CATEGORY

MATHEMATICAL & COMPUTATIONAL BIOLOGY

8/55

JCR YEAR	JIF RANK	QUARTILE	JIF PERCENTILE
2022	8/55	Q1	86.4
2021	18/57	Q2	69.30
2020	31/58	Q3	47.41
2019	39/59	Q3	34.75
2018	40/59	Q3	33.05
2017	54/59	Q4	9.32
2016	48/57	Q4	16.67
2015	44/56	Q4	22.32
2014	52/57	Q4	9.65
2013	47/52	Q4	10.58

Rank by Journal Citation Indicator (JCI)

Journals within a category are sorted in descending order by Journal Citation Indicator (JCI) resulting in the Category Ranking below. A separate rank is shown for each category in which the journal is listed in JCR. Data for the most recent year is presented at the top of the list, with other years shown in reverse chronological order.Learn more

CATEGORY

MATHEMATICAL & COMPUTATIONAL BIOLOGY

15/67

JCR YEAR	JCI RANK	QUARTILE	JCI PERCENTILE
2022	15/67	Q1	78.36
2021	26/68	Q2	62.50
2020	34/67	Q3	50.00
2019	36/66	Q3	46.21
2018	49/64	Q4	24.22
2017	54/64	Q4	16.41

SPRINGER LINK

Log in

Find a journal | Publish with us | Search | Cart

Interdisciplinary Sciences: Computational Life Sciences

Interdisciplinary Sciences: Computational Life Sciences > Volumes and issues > Volume 15, issue 3

Search within journal

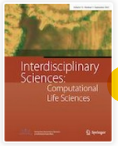

Volume 15, issue 3, September 2023

14 articles in this issue

Complex Prediction in Large PPI Networks Using Expansion and Stripe of Core Cliques

Tushar Ranjan Sahoo, Swati Vipsita & Sabyasachi Patra

Original research article | Published: 28 October 2022

Pages: 331 - 348

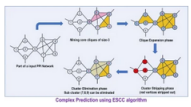

Analysis of CRISPR-Cas Loci and their Targets in *Levilactobacillus brevis*

Ying-Xian Goh, Meng Wang ... Hong-Yu Ou

Original research article | Published: 28 February 2023

Pages: 349 - 359

A Novel Deep-Learning-Based CADx Architecture for Classification of Thyroid Nodules Using Ultrasound Images

Volkan Göreke

Original research article | Published: 28 March 2023

Pages: 360 - 373

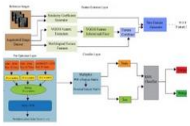

You have access to our articles

For authors

- Submission guidelines
- Language editing services
- Ethics & disclosures
- Open Access fees and funding
- Contact the journal

Submit manuscript

Working on a manuscript?

Avoid the most common mistakes and prepare your manuscript for journal editors

Learn more →

Explore

- Online first articles
- Volumes and issues

Sign up for alerts